Desalination and Water Treatment
www.deswater.com
doi: 10.5004/dwt.2021.26543

210 (2021) 415–429
January

Adsorption of Acid Violet 49 dye from aqueous solution by processed agricultural waste

Umesh B. Deshannavar[a,*], Prasad G. Hegde[a], Pallavi S. Patil[b], Namita Tamburi[a], Ruchi K[a], Apoorva Kolur[a], Abhishek Jadhav[a], Mohanad El-Harbawi[c,*]

[a]*Department of Chemical Engineering, KLE Dr. M. S. Sheshgiri College of Engineering and Technology, Udyambag, Belagavi, 590008, Karnataka, India, emails: deshannavar@gmail.com (U.B. Deshannavar), prasadjihegde@gmail.com (P.G. Hegde), namitatamburi@gmail.com (N. Tamburi); ruchikansagra@gmail.com (Ruchi K.), kolurapoorva@gmail.com (A. Kolur), abhijadhav98.aj@gmail.com (A. Jadhav)*
[b]*Department of Biotechnology Engineering, KIT College of Engineering, Kolhapur, 416234, Maharashtra, India, email: pallavipatil17473@gmail.com*
[c]*Chemical Engineering Department, King Saud University, Riyadh 11421, Saudi Arabia, email: melharbawi@ksu.edu.sa*

Received 8 March 2020; Accepted 7 September 2020

ABSTRACT

In this study, batch adsorption of acid violet 49 (AV49) dye onto thermally activated groundnut shell (AGS) was investigated in aqueous solution. The adsorbent was characterized using Fourier transform infrared, scanning electron microscope equipped with energy dispersive spectroscopy, X-ray diffractometer, BET surface area, and CHNSO analyzer. The effects of solution pH, initial AV49 dye concentration, adsorbent quantity, salinity, and contact time on the removal efficiency of AV49 dye were investigated. The factors influencing dye removal were optimized using the response surface optimization technique. It was observed that the adsorption of AV49 dye onto AGS followed the pseudo-second-order kinetic model with the coefficient of determination (R^2) of 0.999 and a root mean square error of 2.28. The isotherm equation parameters were estimated along with an R^2 for Langmuir and Freundlich isotherms. Based on the R^2 values, it was observed that the experimental data are in close agreement with Langmuir isotherm as compared with Freundlich. The AGS achieved a maximum adsorption capacity of 167, 169, and 172 mg/g at temperatures, 301, 313, and 323 K, respectively. The experimental data revealed that AGS can be used as an adsorbent for the removal of AV49 dye from aqueous solution.

Keywords: Adsorption; Groundnut shell; Acid Violet 49 dye; Isotherm; Kinetic study; Design of experiments

1. Introduction

Water is an important commodity that can become polluted by the prolonged presence of one or more pollutants. Contamination of both groundwater and surface water beyond the cleansing limit of nature requires immediate attention [1]. Wastes from the dye industry, active pharmaceutical ingredients, tanneries, and heavy metals from the electroplating and metal finishing industry, among others, are the major pollutants that affect the quality of both surface and groundwater [2,3]. Dyes are the main contaminants of effluents from various processing industries, such as textiles, paints, ceramics, leather tanneries, cosmetics, pulp, paper, and dye-manufacturing units. The extensive use of dyes results in colored effluents, which affect both aquatic and human life when discharged into water bodies [4]. The discharge of industrial effluents containing dyes and associated chemicals to aquifers poses a major

* Corresponding authors.

environmental pollution challenge as this effluent causes color pollution and is toxic. Water scarcity has necessitated a reduction in industrial water use and effluent generation. Most textile industries are aiming toward zero effluent, and the minimal effluent generated after recycling is used for irrigation purposes [5]. Various effluent treatment methods are practiced, and can be categorized as physical, chemical, and biological [6]. Adsorption is the most effective and successfully practiced physical technique for the treatment of dyeing effluents [7]. The advantages of adsorption are its simple operation, inexpensiveness, lack of sludge formation, and no hazardous byproducts [8,9]. Several researchers have attempted to utilize various materials as alternatives to activated charcoal. The alternative materials that have been tested and proved to be adsorbents with reasonable adsorptive efficiency include industrial wastes, agricultural wastes, and agro-industrial wastes. The alternative agricultural, agro-industrial, and forest-based industrial wastes used as effective adsorbents include sawdust [10–12], *Parthenium* weeds [13], Bengal gram seed husk [14], coconut coir dust [15], *Loofa aegyptiaca* [16], rice husk [17], bagasse [18], cotton stalk [19], among others. Industrial wastes with little or no modification have been found to be promising alternatives for removing dye contaminants from textile processing. Some of the industrial wastes that are used as adsorbents are fly ash [20], blast furnace slag [21], sludge [22], black liquor lignin [23], corn cob [24], Bayer red mud [25], and waste carbon slurry [26]. India has an agrarian economy, and is famous for its spices and spice products. India is one of the major producers of rice, cereals, and spice products, and these amount to 18% of the country's gross domestic product. Additionally, India is the second-largest producer of groundnuts worldwide, and the state of Karnataka is the fourth largest producer in India. The groundnut oil industry produces large quantities of groundnut shells, which are discarded as agro-wastes.

In the present study, groundnut shell agricultural waste was used as an adsorbent for the treatment of AV49 dye from synthetic aqueous solution. The batch adsorption study included the investigation of the effects of solution pH, initial dye concentration, contact time, salinity, and quantity of adsorbent on the AV49 dye removal efficiency. Optimization trials were conducted using the one variable at a time (OVAT) approach. The optimum conditions for maximum dye removal efficiency were obtained using the design of experiments and response surface optimization techniques. The adsorption kinetic study and isotherms were analyzed, and are discussed in Section 3.

2. Materials and experimental methodology

2.1. Reagents

The reagents used during the adsorption studies were KNO_3 for estimation of the point of zero charge (PZC) and HCl and NaOH for adjusting the pH. Chemicals of AR grade obtained from NICE Chemicals (P) Ltd. were used throughout the experimental study. AV49 dye (CAS No.: 1694-09-3; molecular structure: triarylmethane class; molecular formula: $C_{39}H_{40}N_3NaO_6S_2$; molecular weight: 733.87 g/mol) was procured from a local vendor. The molecular structure is depicted in Fig. 1. The stock solution was prepared by dissolving a stoichiometric quantity of AV49 dye in deionized water and diluting to obtain solutions of concentrations of 100 to 200 mg/L.

2.2. Adsorbent

Groundnut shells were collected from the field, cleaned, sun-dried, and ground. The groundnut shell (GS) powder that was passed through a 150 μm sieve and retained on a 75 μm sieve used for the activation process. The GS was heated in the absence of air at 400°C for 4 h. Thermally activated groundnut shell (AGS) was stored in an airtight container. The optical images of GS and AGS were captured with a resolution of 4x by using Nikon eclipse Ti microscope and the photographs of GS and AGS were obtained by using Sony α380 camera are shown in Figs. 2a–d, respectively.

2.3. General adsorption procedure

Experiments were performed in 250 mL Borosilicate (Borosil®) conical flasks. One hundred milliliters of the solution of concentrations of 100 to 200 mg/L was utilized. The solution pH was maintained at 2–10 by adding either 0.1 N NaOH or HCL. 1–5 g/L of AGS was added and the contents were agitated immediately in a rotary shaker (LABLINE, Mumbai, India) for 60 min. Samples were pipetted at 15 min time intervals and centrifuged, and the concentrations of the supernatant layer were analyzed using an ultraviolet-visible spectrophotometer (ELICO-BL 198) at 550 nm. All the experiments were conducted at 28°C.

2.4. Optimization studies using response surface optimization

Batch adsorption tests were designed to determine the maximum dye removal efficiency by the central composite design (CCD) technique using Design-Expert version 10 software to optimize the pH of the solution, adsorbent quantity, and initial dye concentration. The details of the CCD technique are tabulated in Table 1.

3. Results and discussion

3.1. Adsorbent characterization

The raw GS and AGS were analyzed using a scanning electron microscope (SEM) equipped with energy dispersive spectroscopy (EDS) (XL 30 ESEM). The SEM-EDS has been performed at different magnification scale with an accelerating voltage of 30 kV. The morphology of GS and AGS is shown in Fig. 3. SEM images shown in Fig. 3a of GS before activation at 2,200X and Fig. 3b of GS after activation (AGS), on comparison it was observed that the surface morphology of the adsorbent was smooth before the activation process; however, after activation, there was a considerable change in the morphology, which is evident from Fig. 3b. A substantial increase in porosity was observed in the adsorbent sample after activation. These pores play a significant role in the adsorption of the AV49 dye. The EDS spectrum is depicted in Figs. 4 and 5 for both GS and AGS, respectively. The EDS spectrum shown in Figs. 4 and 5 of GS

and AGS, respectively confirmed that the powder is chemically composed of carbon, aluminum, silica, magnesium, and iron. The EDS spectra of AGS showed an increase in percentage of carbon. However, the elemental composition of aluminum, silica, magnesium, and iron has not significantly changed in GS and AGS.

The X-ray diffractometer (XRD) data from the Rigaku Smart Lab X-ray diffractometer (Tokyo, Japan) was used to analyze and characterize the composition of the adsorbent. The values of intensity of 2θ were plotted within an angle range of 5° to 90°, and the scanning speed was set to 4°/min. Fig. 6 shows the XRD peaks for GS and AGS. The peak positions of GS and AGS did not change. The highest peak was recorded at a 2θ value of 26.7 and a minor peak at 54.79, both peaks matched with Joint Committee on Powder Diffraction Standards (JCPDS) card no. 261079, which is of carbon. The highest intensity of carbon in XRD is in close agreement with EDS data of AGS where carbon percentage is seen more. A minor peak of iron oxide was seen at a 2θ value of 19.8 (JCPDS card no. 760955). The peak of silica is seen at 20.97 (JCPDS card no. 862364). Similarly, aluminum oxide, magnesium oxide peaks were seen at 35.6, 45.93, and 42.61, respectively, which matched with JCPDS card no. 851337, 750921 of aluminum oxide, and 190771 of magnesium oxide, respectively. The elemental compositions are in close agreement based on the analysis of XRD and SEM-EDS spectra.

The Fourier-transform infrared spectroscopy (FTIR) (Nicolet, 6700 USA) of AGS before and after AV49 dye adsorption studies was performed and shown in Fig. 7. Fourier transform infrared spectral analysis enabled the identification of the functional group and molecular structure of the AGS. Spectra obtained from 40 to 4,000 cm^{-1}

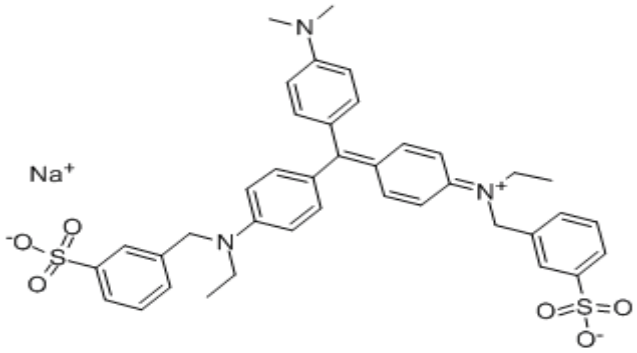

Fig. 1. Molecular structure of Acid Violet 49 (AV49) dye.

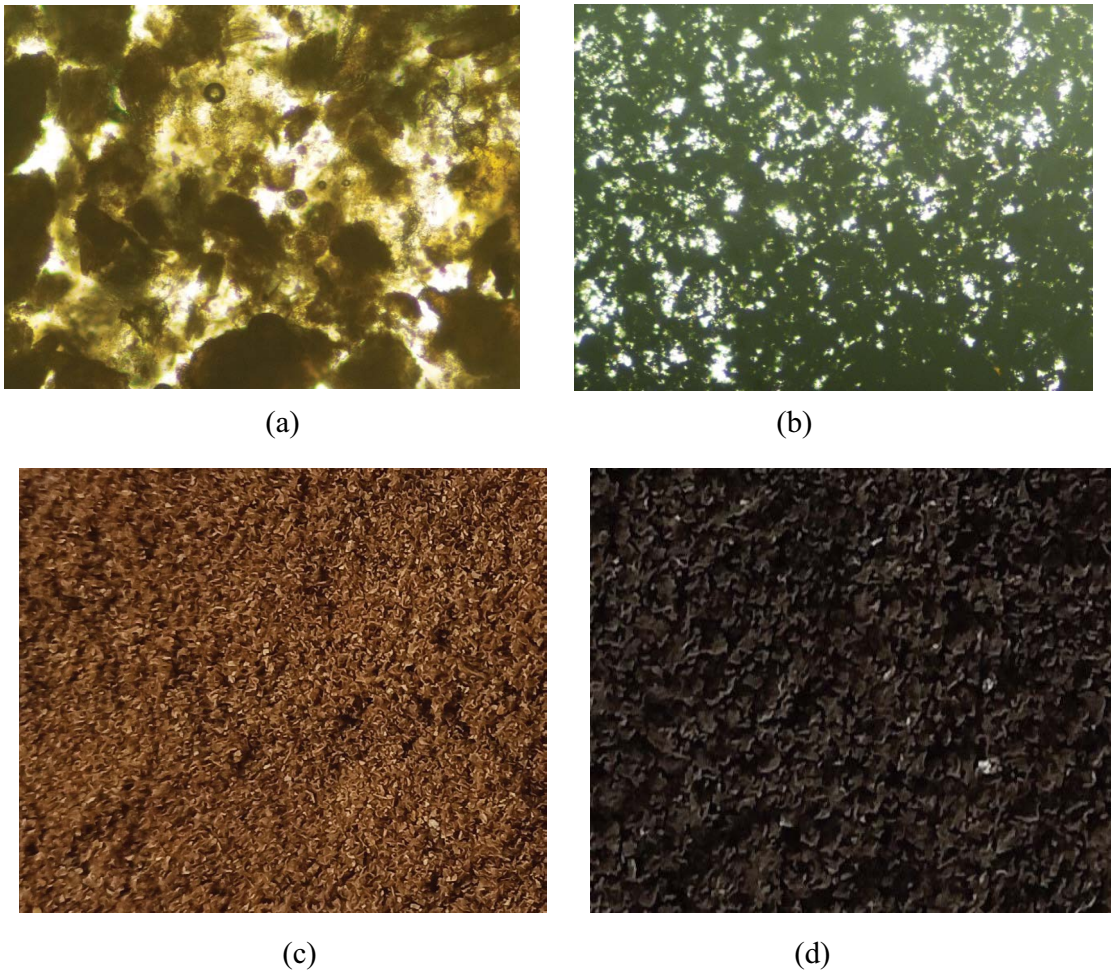

Fig. 2. Optical images of (a) GS (b) AGS and photographs of (c) GS and (d) AGS.

Table 1
Summary of the batch adsorption conditions using response surface optimization

Run No.	pH (–)	Dosage (g/L)	Concentration (mg/L)
1	2.0	2.0	150
2	3.0	1.5	125
3	2.0	1.0	100
4	3.0	1.5	125
5	3.0	2.3	125
6	4.0	1.0	100
7	4.7	1.5	125
8	3.0	0.7	125
9	4.0	2.0	150
10	3.0	1.5	125
11	3.0	1.5	83
12	4.0	1.0	150
13	2.0	2.0	100
14	4.0	2.0	100
15	1.3	1.5	125
16	3.0	1.5	125
17	2.0	1.0	150
18	3.0	1.5	167
19	3.0	1.5	125
20	3.0	1.5	125

were recorded at 4 cm^{-1} nominal resolution with mathematical corrections yielding a 1.0 cm^{-1} actual resolution. The vibrational spectrum has several specific absorption bands caused by different functional groups. Peaks were observed at 3,363.78; 1,714.91; 1,570.27; 1,222.49; and 1,010.65 cm^{-1}. 3,200–3,600 cm^{-1} indicates the presence of several functional groups namely O–H alcohol group, amino, carboxylic, phosphate, and sulfonate on the AGS surface. The prominent O–H alcohol group is indicated by broad and intense peak at 3,363.78 cm^{-1}. The amine group N–H and N–H_2 are less broad and less intense than O–H group stretch. Carboxylic C=O stretch is strong and generally appears in between 1,650 and 1,850 cm^{-1}. In the FTIR of AV49 ($C_{39}H_{40}N_3NaO6S_2$) adsorbed on AGS is observed at 3,363.78 cm^{-1}, which indicates the presence of O–H group. The hydroxyl, carboxyl, and amine groups at the surface of AGS indicated by peaks help in the adsorption of AV49 from aqueous solution. The carbon, hydrogen, nitrogen, sulfur, and oxygen (CHNSO) and surface area analyses of both the GS and AGS were performed using a CHNS-O Analyzer (Thermo Fisher, USA) and the Brunauer–Emmett–Teller (BET) method, respectively, and the results are summarized in Table 2. The BET surface areas of the GS and AGS were determined to be 475 and 1,325 m^2/g, respectively. The increase in the surface area of the AGS was due to the effect of temperature in the absence of air [27]. At higher temperatures, volatile matter and tars of GS are released, thereby leaving behind the porous structure of carbon. The carbonaceous content of GS underwent incomplete combustion in the absence of air and was converted into char as a result of the breakdown of the lignocellulosic content. Thus, the fixed carbon content and organic carbon content of AGS were higher compared with those of GS [27].

3.2. Point of zero charge

The PZC indicates the pH value at which the surface of the adsorbent has zero charge. The PZC of the adsorbent was evaluated according to the procedure followed by Ofomaja and Ho [28]. If the solution pH < PZC, then the surface of the adsorbent will be positively charged and adsorb anions. If pH > PZC, then cations are adsorbed on the adsorbent surface owing to the presence of a negative charge. Fig. 8 shows the PZC for AGS. The PZC of AGS was 7.55.

3.3. Solution pH

The amenability of charges on the adsorbent surface depends on the pH of the AV49 dye solution. Experiments were conducted to investigate the effect of solution pH by varying the pH from 2 to 10 in increments of 2. It was

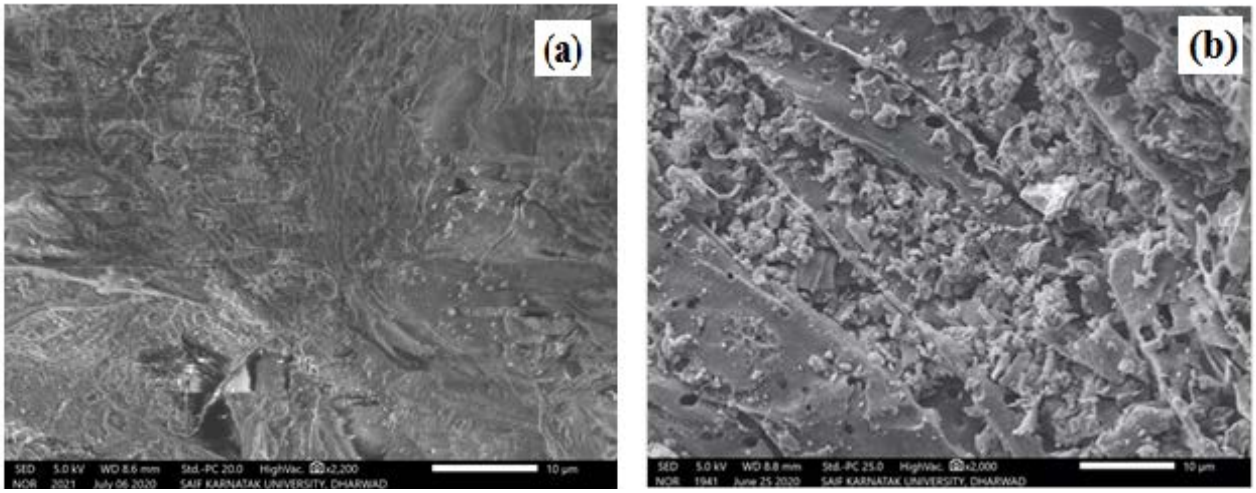

Fig. 3. SEM images of (a) GS and (b) AGS.

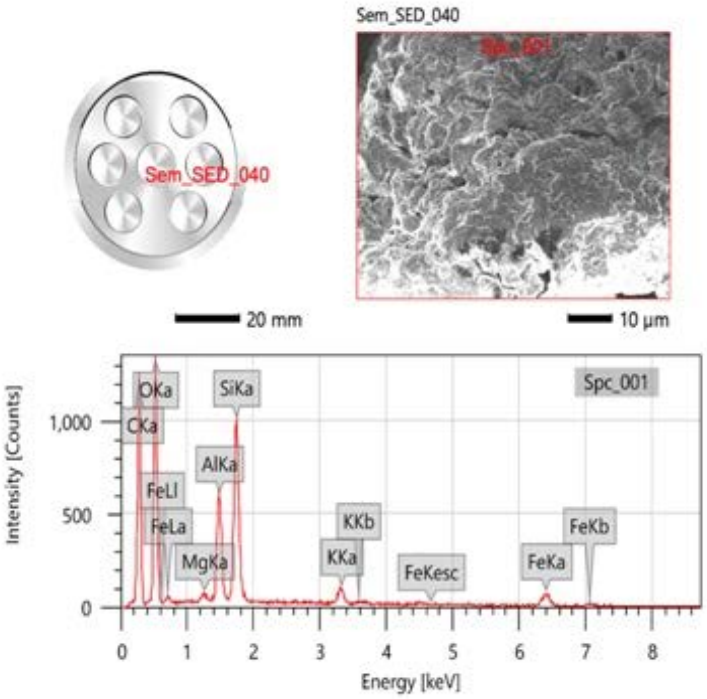

Signal SED
Landing Voltage 5.0 kV
WD 8.7 mm
Magnification x1,800
Vacuum Mode HighVacuum

Items	Value
measurement conditions	
Acceleration voltage	20.00 kV
Probe current	0.00 nA
Magnification	x 1800
Process time	T3
Measurement detector	First
Live time	30.00 seconds
Real time	30.39 seconds
Dead time	1.00
Count rate	1418.00 CPS

Display name	Standard data	Quantification method	Result Type
Spc_001	Standardless	ZAF	Metal

Element	Line	Mass%	Atom%
C	K	40.92±0.21	50.98±0.26
O	K	45.15±0.39	42.23±0.37
Mg	K	0.30±0.03	0.18±0.02
Al	K	3.89±0.07	2.16±0.04
Si	K	6.51±0.09	3.47±0.05
K	K	0.93±0.04	0.35±0.01
Fe	K	2.30±0.08	0.62±0.02
Total		100.00	100.00
Spc_001			Fitting ratio 0.0283

Fig. 4. EDS of GS.

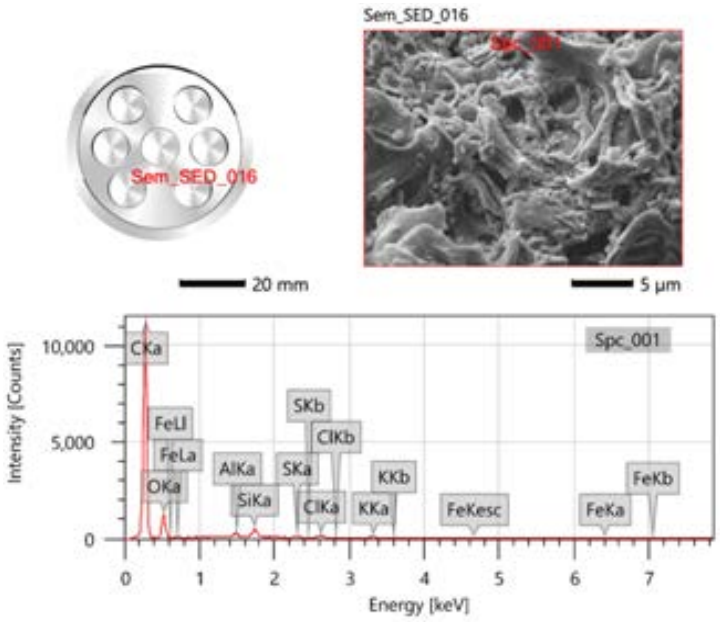

Signal SED
Landing Voltage 5.0 kV
WD 8.9 mm
Magnification x5,000
Vacuum Mode HighVacuum

Items	Value
measurement conditions	
Acceleration voltage	20.00 kV
Probe current	0.00 nA
Magnification	x 5000
Process time	T3
Measurement detector	First
Live time	30.00 seconds
Real time	30.70 seconds
Dead time	2.00
Count rate	3641.00 CPS

Display name	Standard data	Quantification method	Result Type
Spc_001	Standardless	ZAF	Metal

Element	Line	Mass%	Atom%
C	K	71.63±0.12	77.95±0.13
O	K	25.74±0.23	21.03±0.19
Al	K	0.46±0.02	0.22±0.01
Si	K	0.92±0.02	0.43±0.01
S	K	0.12±0.01	0.05±0.00
Cl	K	0.29±0.01	0.11±0.00
K	K	0.21±0.01	0.07±0.00
Fe	K	0.64±0.03	0.15±0.01
Total		100.00	100.00
Spc_001			Fitting ratio 0.0153

Fig. 5. EDS of AGS.

found that 92% of the AV49 dye was removed at the solution pH of 2 (Fig. 9). At lower pH values, the adsorbent surface acquired a positive charge and favored negatively charged AV49 anions. As the pH increased, the degree of adsorption decreased. A low dye removal efficiency of 15% was observed at a higher pH value of 10. Thus, as the solution pH increased, the negatively charged sites on the AGS surface repelled negatively charged dye anions.

3.4. Initial Acid Violet 49 dye concentration and contact time

In order to investigate the effects of the initial dye concentration and adsorbate–adsorbent contact time on the AV49 removal efficiency, batch adsorption trials were conducted by changing the initial dye concentration range from 100 to 200 mg/L. The contents were drawn at every 15 min of agitation time and analyzed for the final dye

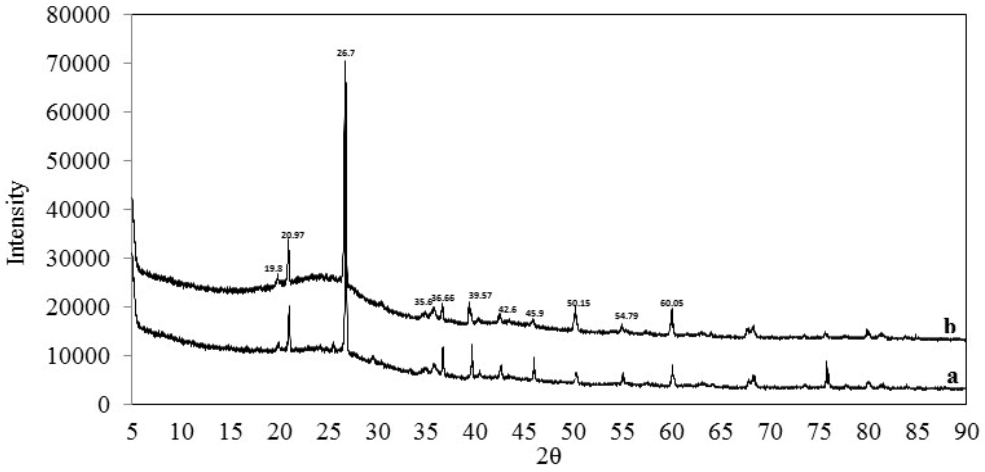

Fig. 6. XRD of (a) GS and (b) AGS.

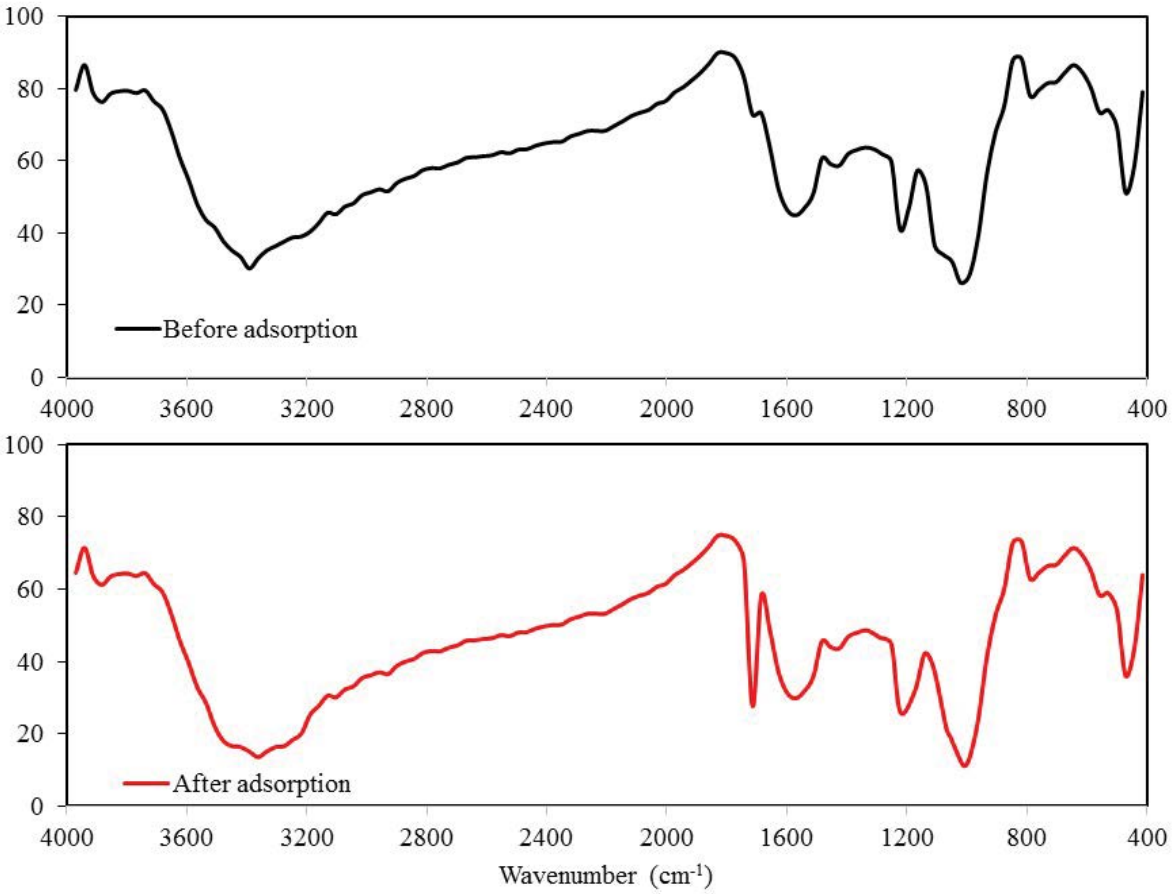

Fig. 7. FTIR spectra of AGS.

concentration. It was found that the AV49 dye removal efficiency decreased with the increase in the initial dye concentration (Fig. 10), whereas the amount adsorbed at equilibrium increased with the increase in the initial AV49 dye concentration (Fig. 11). For 100 mg/L of AV49 dye, 92% removal (amount adsorbed = 92 mg/g) was achieved, whereas for 150 and 200 mg/L of AV49 dye, removal efficiencies of 86% (amount adsorbed = 129 mg/g) and 74% (amount adsorbed = 149 mg/g), respectively, were achieved after 60 min of agitation. It was also observed that the amount of dye adsorbed onto AGS increased with the increase in contact time and reached equilibrium after 60 min of

Table 2
Surface area and carbon, hydrogen, nitrogen, and sulfur contents of groundnut shell (GS) powder and activated groundnut shell (AGS)

Property	Value	
	GS	AGS
BET surface area, m^2/g	475	1,325
C, %	33.59	36.40
H, %	3.38	7.99
N, %	0.92	1.03
S, %	0.28	0
O, %	61.80	54.57

agitation. The maximum dye adsorption/removal efficiency was achieved after 15 min of agitation. The rate of change of AV49 dye adsorption with time attains a plateau and there is no significant increase in adsorption beyond 60 min of contact between adsorbate and adsorbent.

3.5. Kinetic study

The kinetic adsorption data help to understand the dynamics of the adsorption process in terms of the order of the rate constants. The equations used for the kinetic study were the Lagergren pseudo-first-order, pseudo-second-order, and intra-particle diffusion (IPD). The linear form of the Lagergren pseudo-first-order equation is as follows [29]:

$$\log\left(q_e - q\right) = \log q_e = \frac{K_1 t}{2.303} \tag{1}$$

where q (mg/g) is amount of dye adsorbed at time t (min), q_e (mg/g) is amount of dye adsorbed at equilibrium time, and K_1 (min^{-1}) is pseudo-first-order rate constant.

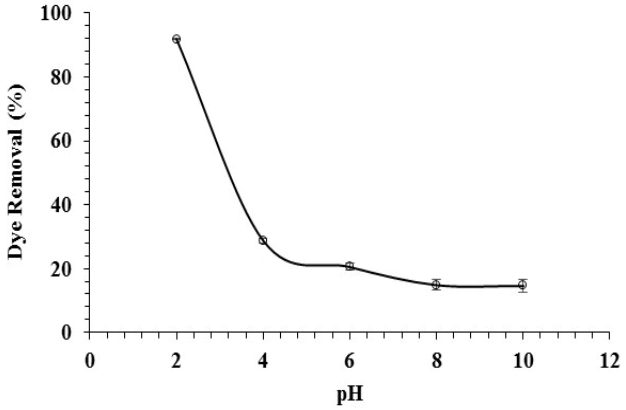

Fig. 9. Effect of solution pH on AV49 dye removal efficiency (dye concentration = 100 mg/L; adsorbent dosage = 1 g/L; agitation time = 60 min; pH = 2–10, standard deviation: 0.15 to 2.13).

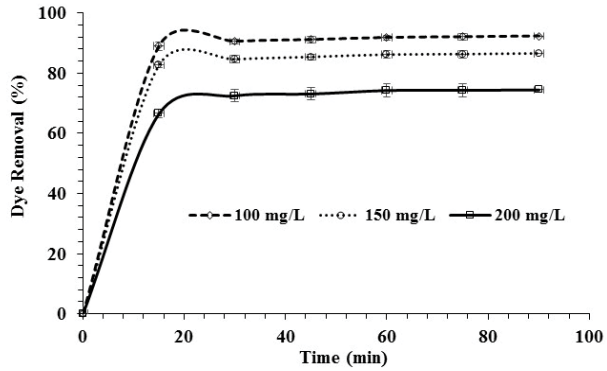

Fig. 10. Effect of initial dye concentration and contact time on AV49 dye removal efficiency (dye concentration = 100–200 mg/L; adsorbent dosage = 1 g/L; pH = 2, standard deviation: 0.79 to 2.32).

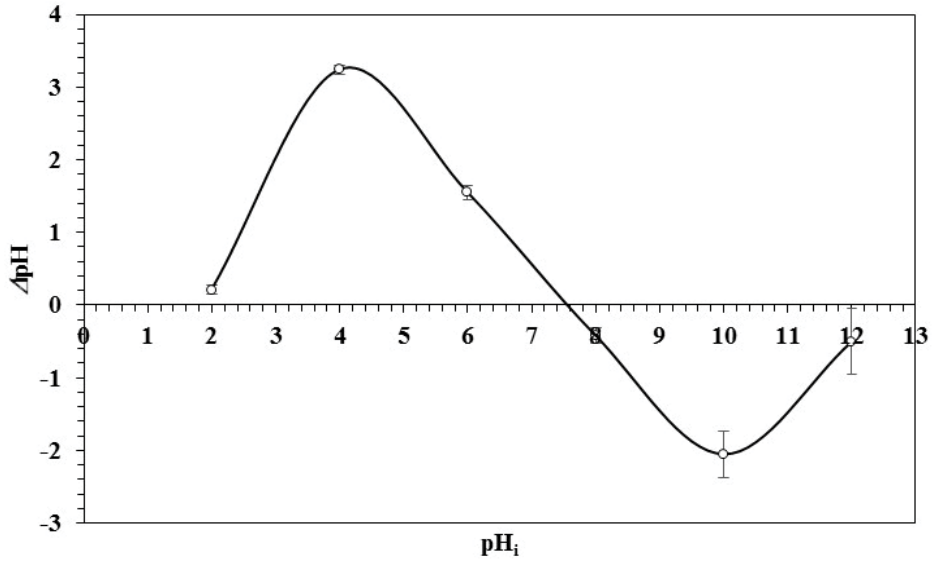

Fig. 8. Point of zero charge of activated groundnut shell (standard deviation: 0.06 to 0.45).

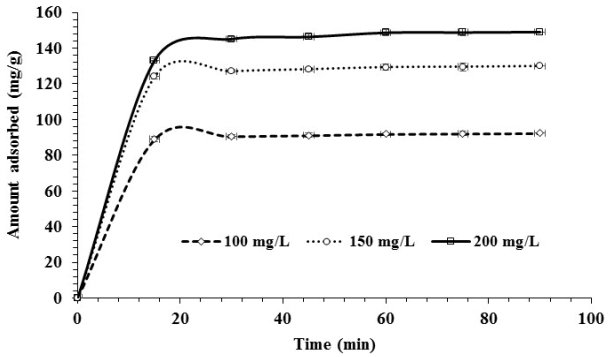

Fig. 11. Effect of initial dye concentration and contact time on AV49 dye adsorption at equilibrium (dye concentration range = 100–200 mg/L; pH = 2; adsorbent dosage = 1 g/L, standard deviation: 0.79 to 2.68).

The linear form of the pseudo-second-order equation is as follows [30]:

$$\frac{t}{q} = \frac{1}{K_2 q_e^2} + \frac{t}{q_e} \tag{2}$$

where K_2 (g mg^{-1} min^{-1}) is pseudo-second-order rate constant.

The linear form of the intra-particle diffusion model is [31]:

$$q = k_p t^{1/2} + C \tag{3}$$

where k_p is IPD rate constant (mg/(g min$^{1/2}$)) and C is a constant (mg/g) associated with the thickness of boundary layer.

Pseudo-first-order, second-order, and IPD kinetic model parameters were determined by plotting log (q_e-q) vs. t (Fig. 12), t/q vs. t (Fig. 13), and q vs. $t^{1/2}$ (Fig. 14), respectively. The model parameters estimated along with the coefficient of determination (R^2) value and root mean square error (RMSE) are tabulated in Table 3. However, the R^2 values of the pseudo-first-order and pseudo-second-order plots were above 0.9, and the values of q_e calculated by the experiment and by the pseudo-first-order kinetic model showed a significant difference. The adsorption of AV49 dye onto AGS followed the pseudo-second-order kinetic model with an R^2 value almost 1 and RMSE of 2.28. The intra-particle diffusion is considered as a rate controlling step in the adsorption study if the lines of the plot q vs. $t^{1/2}$ pass through the origin [31]. In Fig. 14, the lines did not pass through the origin indicating that the IPD is involved in the adsorption process but is not the rate controlling step. The IPD plot (Fig. 14) is divided into two zones: the first zone represents the intra-particle diffusion whereas, the second zone represents the slow equilibrium.

3.6. Adsorption isotherms

Different isotherm models have been used to study the adsorption equilibrium. Langmuir and Freundlich isotherm equations are commonly accepted and used to estimate the adsorption potential of adsorbents. The Langmuir equation in linear form is as follows [32]:

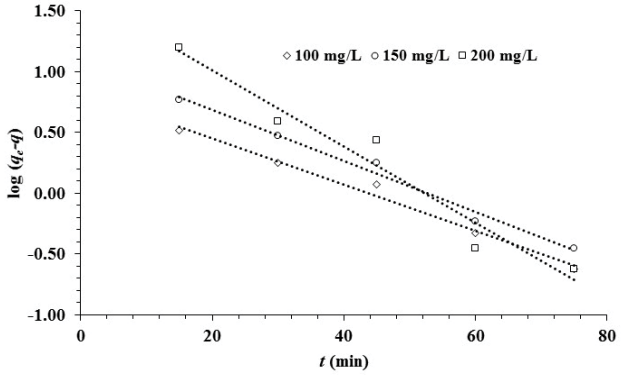

Fig. 12. Pseudo-first-order kinetics for the adsorption of AV49 dye onto activated groundnut shell (dye concentration = 100–200 mg/L; adsorbent dosage = 1 g/L; solution pH = 2).

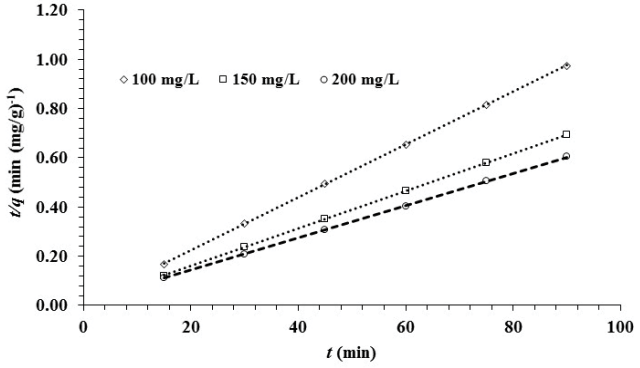

Fig. 13. Pseudo-first-order kinetics for the adsorption of AV49 dye onto activated groundnut shell (dye concentration = 100–200 mg/L; adsorbent dosage = 1 g/L; solution pH = 2).

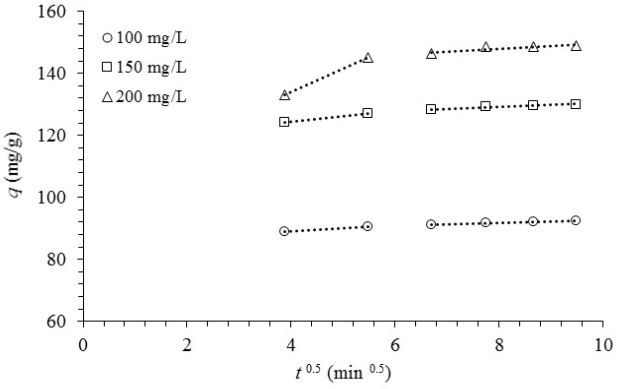

Fig. 14. Intra-particle diffusion kinetics for the adsorption of AV49 dye onto activated groundnut shell (dye concentration = 100–200 mg/L; adsorbent dosage = 1 g/L; solution pH = 2).

$$\frac{C_e}{q_e} = \frac{1}{Q_0 b} + \frac{C_e}{Q_0} \tag{4}$$

where C_e (mg/L) is equilibrium concentration of dye, Q_0 (mg/g) is adsorption capacity and b (L/mg) is constant.

Table 3
Pseudo-first-order, pseudo-second-order, and IPD kinetic model parameters

Dye concentration (mg/L)	Experiment $q_e^{\#}$ (mg/g)	Pseudo-first-order kinetic model parameters				Pseudo-second-order kinetic model parameters				Intra-particle diffusion model parameters		
		K_1^{+} (min^{-1})	$q_e^{\#}$ (mg/g)	R^2	RMSE	K_2^{++} ($g \cdot mg^{-1} min^{-1}$)	$q_e^{\#}$ (mg/g)	R^2	RMSE	k_p^{+++} (mg/(g $min^{1/2}$))	$C^{\$}$ (mg/g)	R^2
100	91.86	0.044	6.87	0.9863		0.014	93.46	1.000		0.58	87.12	0.80
150	129.35	0.048	12.72	0.9861	103.15	0.008	131.58	1.000	2.28	1.03	120.81	0.93
200	148.68	0.072	43.35	0.9542		0.004	151.52	0.999		2.55	127.36	0.95

$^{\#}$Amount adsorbed at equilibrium time, $^{+}$pseudo-first-order rate constant, $^{++}$pseudo-second-order rate constant, $^{+++}$IPD rate constant, $^{\$}$Constant.

The dimensionless constant R_L is estimated as follows:

$$R_L = \frac{1}{1 + bC_0} \tag{5}$$

where C_0 (mg/L) is initial dye concentration. The values of R_L ranging from 0 to 1 indicate favorable adsorption [33].

The Freundlich equation in linear form is expressed as follows [34]:

$$\log q_e = \log K_F + \frac{1}{n} \log C_e \tag{6}$$

where K_F (mg/g) is adsorption capacity and n is constant. The values of n between 1 and 10 indicate favorable adsorption [35].

The plots of C_e/q_e vs. C_e and log q_e vs. log C_e are shown in Figs. 15 and 16 at 301, 313, and 323 K, respectively. The isotherm equation parameters estimated along with R^2 values are summarized in Table 4 for both Langmuir and Freundlich isotherms. It was observed that the R_L value ranged from 0 to 1 and n was in the range from 1 to 10. Based on the R^2 values, it was concluded that experimental data fit well with Langmuir isotherm as compared with Freundlich. It is also observed that maximum adsorption capacities increased with an increase in temperature indicating that the adsorption process is enhanced with temperature rise. Similar observations were also made by Mane and Babu [36] for congo red dye removal using Eucalyptus wood (*Eucalyptus globulus*) saw dust.

3.7. Adsorbent dosage

The quantity of adsorbent affects the adsorption of AV49 dye onto AGS. In order to study the effect of the adsorbent quantity on dye adsorption, experiments were performed with varying adsorbent quantities from 1 to 5 g/L. AV49 dye adsorption on AGS increased with an improvement in adsorbent quantity up to 1 g/L (Fig. 17). This was mainly owing to the accessibility of adequate adsorption sites and enhanced surface area with the increase in adsorbent quantity. The maximum dye removal of 92% was achieved with the adsorbent quantity of 1 g/L. A further increase in adsorbent quantity did not result in a significant increase in dye removal. This might have been attributed to the overlapping of active sites of the adsorbent particles.

Table 4
Langmuir and Freundlich isotherm constants

Isotherm	Parameter	301 K	313 K	323 K
Langmuir	Q_0* (mg/g)	167	169	172
	b** (L/mg)	0.16	0.12	0.08
	R_L	0.06	0.08	0.11
	R^2	0.9998	0.9994	0.999
Freundlich	K_F* (mg/g)	54.8	47.1	37.7
	n**	3.82	3.44	2.99
	R^2	0.9469	0.9476	0.9567

*Adsorption capacity, **constant.

3.8. Effect of salt concentration

The effect of salt concentration on adsorption capacity of AGS was investigated by using sodium chloride (NaCl). The salt concentration raised from 0% to 10% (W/V). The batch adsorption experiments were conducted at optimum conditions. Langmuir and Freundlich isotherm models were used to describe the process. The plots of C_e/q_e vs. C_e and log q_e vs. log C_e are shown in Figs. 18 and 19 at 301 K, respectively. The isotherm equation parameters estimated along with R^2 values are summarized in Table 5 for both Langmuir and Freundlich isotherms. It was observed that the maximum adsorption capacities decreased with an increase in salt concentration from 0% to 10%. An increase in ion strength of sodium ions in a solution leads to a decrease in active binding sites and hence the adsorption capacity. The reduction in adsorption capacity is attributed to competition between ions of similar charge [37].

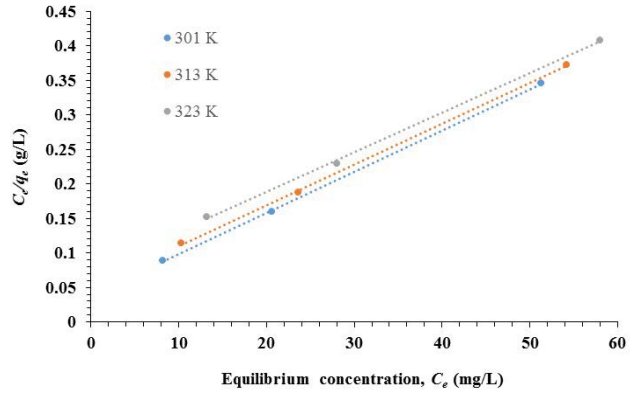

Fig. 15. Linear Langmuir adsorption isotherm (dye concentration = 100–200 mg/L; adsorbent dosage = 1 g/L; agitation time = 60 min; pH = 2, temperature = 301–323 K).

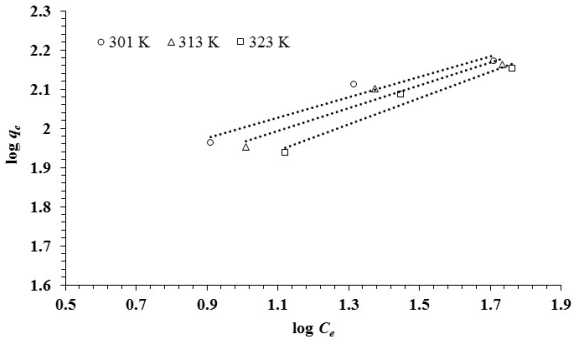

Fig. 16. Linear Freundlich adsorption isotherm (dye concentration = 100–200 mg/L; adsorbent dosage = 1 g/L; agitation time = 60 min; pH = 2, temperature = 301–323 K).

3.9. Design of experiments and response surface optimization

According to the experimental data obtained from the adsorption studies, the (–1) and (+1) values of the three parameters, namely solution pH, adsorbent dosage, and initial dye concentration, were set as 2 and 4; 1 and 2 g/L; and 100 and 150 mg/L, respectively. It was observed from the experimental data that equilibrium was attained after 60 min of contact between the adsorbate and adsorbent. Thus, contact time was not considered one of the input parameters for optimization. A set of 20 experiments designed according to the CCD technique were conducted following the general adsorption procedure mentioned in Section 2.3 to determine the effect of the three parameters at room temperature. Response surface methodology helps to determine the effect of these variables individually and that of their interaction on dye removal efficiency, and also helps to identify the optimum conditions. The set of experiments with actual and predicted dye removal efficiency are presented in Table 6. The mathematical equation that predicted the AV49 dye removal efficiency in terms of coded factors generated by analysis of variance (ANOVA) is given as follows:

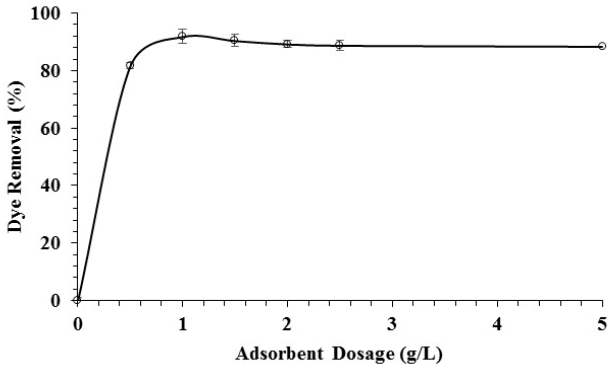

Fig. 17. Effect of adsorbent dosage on dye removal efficiency (dye concentration = 100 mg/L; adsorbent dosage = 1–5 g/L; pH = 2; agitation time = 60 min, standard deviation: 1.11 to 2.40).

Table 5
Langmuir and Freundlich isotherm constants at various salt concentrations

NaCl (%, W/V)	Langmuir parameter			Freundlich parameter		
	Q_0* (mg/g)	b** (L/mg)	R^2	K_F* (mg/g)	n**	R^2
0	167	0.16	0.998	54.8	3.82	0.9469
5	161	0.13	0.997	50.4	3.80	0.9483
10	159	0.11	0.994	45.8	3.63	0.9449

*Adsorption capacity, **constant.

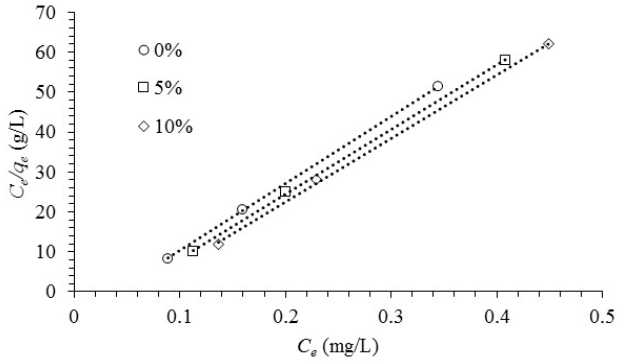

Fig. 18. Linear Langmuir adsorption isotherm (dye concentration = 100–200 mg/L; adsorbent dosage = 1 g/L; agitation time = 60 min; pH = 2, salt concentration = 0–10% (W/V), temperature = 301 K).

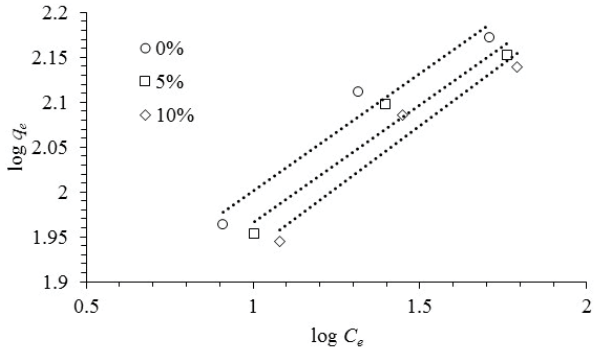

Fig. 19. Linear Freundlich adsorption isotherm (dye concentration = 100–200 mg/L; adsorbent dosage = 1 g/L; agitation time = 60 min; pH = 2, salt concentration = 0–10% (W/V), temperature = 301 K).

$$\text{Dye Removal} = 58.96 - 19.33 \times A - 2.20 \times B - 3.50 \times C + 1.25 \times AB + 2.00 \times AC - 0.25 \times BC + 0.46 \times A^2 - 0.068 \times B^2 + 0.11 \times C^2 \quad (7)$$

The coefficients of *A* (pH) and *C* (concentration) were negative, thereby indicating that with an increase in solution pH and initial dye concentration, the AV49 dye removal decreased. Meanwhile, the coefficient of adsorbent dosage (*B*) was positive, which indicated an increase in dye removal with the increase in adsorbent dosage. The R^2, adjusted R^2, and predicted R^2 values were 0.9944, 0.9894, and 0.9678, respectively. A *p*-value of <0.0001 implied that the model is significant (Table 7). Based on the ANOVA, the solution pH (*A*), initial dye concentration (*C*), interaction between solution pH and adsorbent dosage (*AB*), and interaction between solution pH and initial dye concentration (*AC*) were significant model terms. Thus, the 3D surface plots of the combined effects of *AB* and *AC* are shown in Figs. 20 and 21, respectively. The optimum values are shown in Table 8.

Table 6
Actual and predicted values of dye removal efficiency

Run No.	pH (–)	Dosage (g/L)	Concentration (mg/L)	Dye removal (%) Actual	Predicted
1	2.0	2.0	150	71	70
2	3.0	1.5	125	59	58
3	2.0	1.0	100	91	90
4	3.0	1.5	125	58	58
5	3.0	2.3	125	62	62
6	4.0	1.0	100	42	41
7	4.7	1.5	125	28	28
8	3.0	0.7	125	58	60
9	4.0	2.0	150	37	37
10	3.0	1.5	125	60	58
11	3.0	1.5	83	65	66
12	4.0	1.0	150	35	34
13	2.0	2.0	100	88	87
14	4.0	2.0	100	48	48
15	1.3	1.5	125	92	94
16	3.0	1.5	125	60	58
17	2.0	1.0	150	75	73
18	3.0	1.5	167	45	46
19	3.0	1.5	125	57	58
20	3.0	1.5	125	57	58

3.10. Adsorption mechanism

The adsorption mechanism of AV49 dye onto AGS can be explained based on the electrostatic attraction between the dye and AGS. This can be explained by pH dependence of the adsorption of adsorbate onto adsorbent. When the solution pH was 2, the AGS possessed positively charged surface and thus attracts anionic AV49 dye and results in increasing dye removal percentage (maximum dye adsorption). On the other hand, as solution pH increases, the dye removal efficiency decreases as the repulsion between AV49 dye and AGS increases because of negatively charged AGS surface. Hence it is clear that most of the AV49 dye uptake processes involve electrostatic force of attraction.

Based on the adsorption kinetic study, it appears that the adsorption kinetics data fit the pseudo-second-order model marginally better than the pseudo-first-order model, implying the existence of both physisorption and chemisorption as the overarching sorption mechanism. The slightly higher R^2 value for pseudo-second-order model would suggest that chemisorption is the rate-controlling step [38,39], though this might be minor.

Based on the isotherm analysis, our sorption data fit the Langmuir model slightly better than the Freundlich model, judging by the higher R^2 value for the former. This equilibrium observation is consistent with our kinetics findings in preceding section in which chemisorption is marginally more prominent than physisorption but this supports the notion that both mechanisms are in play in the adsorption system. As such, it is surmised that there could be a combination of monolayer (chemisorption) and multilayer

Table 7
Analysis of variance results

Source	Sum of squares	df[e]	Mean square	*F*-value	*p*-value Prob > *F*
Model	5,879.36	9	653.26	198.91	<0.0001 (significant)
A (pH)	5,284.13	1	5,284.13	1,608.98	<0.0001
B (dosage)	6.93	1	6.93	2.11	0.1770
C (concentration)	500.02	1	500.02	152.25	<0.0001
AB	21.13	1	21.13	6.43	0.0296
AC	21.13	1	21.13	6.43	0.0296
BC	6.13	1	6.13	1.87	0.2020
A^2	14.88	1	14.88	4.53	0.0592
B^2	14.88	1	14.88	4.53	0.0592
C^2	8.14	1	8.14	2.48	0.1464
Residual	32.84	10	3.28		
Lack of fit	23.34	5	4.67	2.46	0.1732 (not significant)
Pure error	9.50	5	1.90	198.91	<0.0001
Cor. total	5,912.20	19			

[e]Degree of freedom.

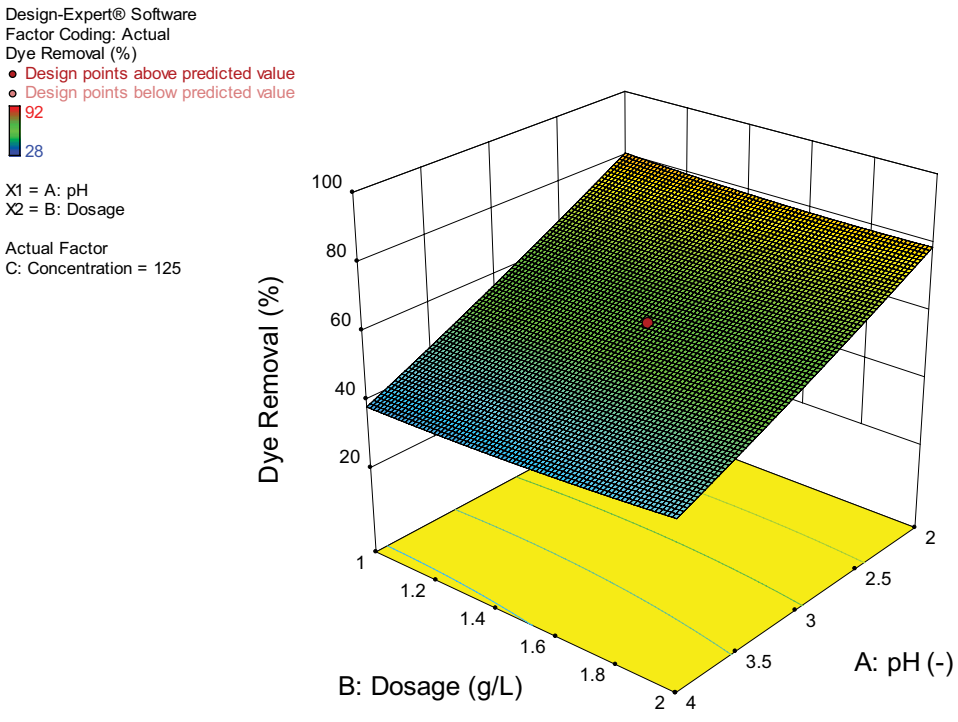

Fig. 20. Surface plot of the effect of pH and dosage on dye removal.

(physisorption) adsorption of dye molecules on the surface of the sorbent.

Adsorption mechanisms are proposed based on chemical, morphological, textural characterization, and FTIR spectra. AGS is a carbonaceous adsorbent possessing atomic structure ($1s^2$, $2s^2$, $2p^2$), with a disordered microstructure, and exhibiting exemplary bonding possibilities. Thermal activation enhances the surface chemistry which leads to higher interactions and increased adsorption capacity of the activated carbon. The prominent mechanisms in adsorption by activated carbons are π–π interaction and hydrogen bonding [40]. FTIR data indicate the displacement of the OH group from 3,400 to 3,200 cm^{-1} reflecting the hydrogen bond between the adsorbate and adsorbent hydroxyl groups. The shift of broad band from 3,392.70 to 3,363.78 cm^{-1} could be assigned to the $–NH_2$ asymmetric stretch of amines and bonded –OH groups. A peak at 1,714.91 indicates C=O stretching. The shift of the peak from 1,541.35 to

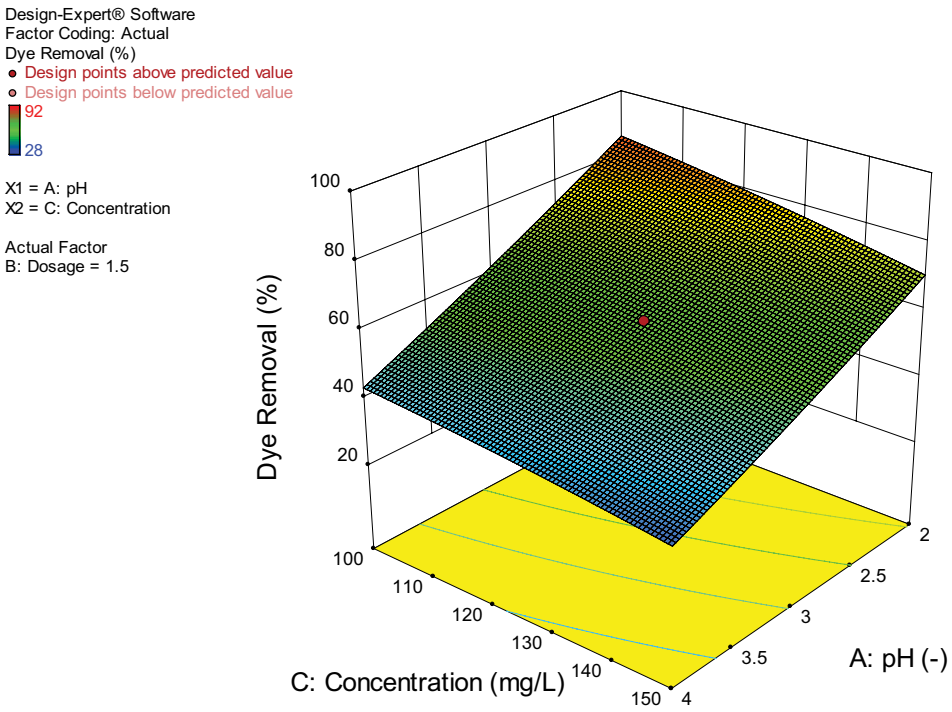

Fig. 21. Surface plot of the effect of pH and dye concentration on dye removal.

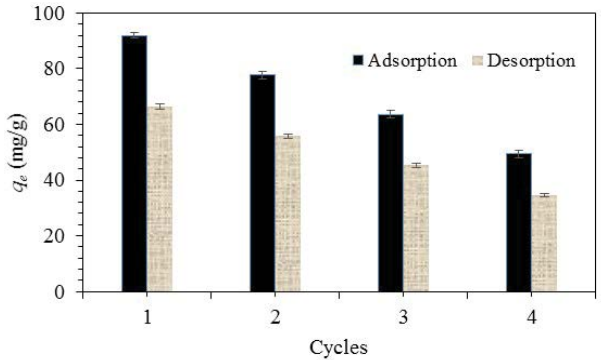

Fig. 22. AGS regeneration for AV49 dye adsorption (standard deviation: 0.61 to 1.32).

Table 8
Optimization results for the Acid Violet 49 dye concentration of 100 mg/L

Parameter	Value
Solution pH (–)	2
Adsorbent dosage (g/L)	1
Contact time (min)	60

1,570.27 cm^{-1} suggests the influence of aromatic rings, favoring the π–π interaction between adsorbent and adsorbate. A number of peaks in the range of 800 to at 400 cm^{-1} confirm the adsorption of AV49 on AGS pores as there is a change in intensity after the adsorptive process which refer to the C–O–C, C=C, and CO– bonds. Adsorption bands between 800 and 600 cm^{-1} may be attributed to aromatic –CH symmetric bending vibrations. The shift in band position and the intensity of peaks after adsorption confirmed that the functional groups on the AGS interact with the dye molecules and were responsible for AV49 adsorption on AGS. To summarize, the main adsorption mechanisms in the present studies were hydrogen bonding and π–π interactions, which corroborates their characterization, in addition to the effect of pH and ionic strength.

3.11. Desorption and regeneration study

In order to evaluate the regeneration capacity of AGS, eluents, NaOH (0.1 M), HCl (0.1 M), deionized water, and ethanol (50% v/v) were tested. The desorption capacity of AGS for AV49 dye was found to be 12.56, 1.20, 0.74, and 66.42 mg/g, respectively. It is found that ethanol exhibits a higher desorption capacity. Adsorption/desorption cycles were carried out with ethanol as eluent to ascertain the possibility of recycling/reuse of AGS (Fig. 22). It is interpreted from Fig. 22 that the adsorption and desorption capacities decreased over four cycles ranging from 92.00 to 49.4 mg/g and 66.4 to 34.68 mg/g which implies 54% and 52.2%, respectively.

4. Conclusions

The factors influencing the AV49 dye adsorption onto AGS were investigated using batch adsorption experiments and optimized using response surface optimization. A maximum dye removal of more than 90% was achieved at an

adsorbent quantity of 1 g/L, pH of 2, and contact time of 60 min for 100 mg/L of AV49 dye. Adsorption kinetic study reveals that AV49 dye adsorption is due to culmination of both physisorption and chemisorption. The Langmuir adsorption isotherm model fits well. Equilibrium observations are in line with kinetic findings and chemisorption is the rate-controlling factor and marginally more prominent than physisorption. SEM and FTIR analysis indicate the presence of AV49 dye on AGS.

Acknowledgments

The authors gratefully acknowledge KLE Dr. M. S. Sheshgiri College of Engineering and Technology, Belagavi for providing the facilities and financial support for conducting this research. M. El-Harbawi also extends his appreciation to the Deanship of Scientific Research at King Saud University for supporting him through research group no. RGP-303.

References

[1] A. Bhatnagar, M. Sillanpää, Utilization of agro-industrial and municipal waste materials as potential adsorbents for water treatment—a review, Chem. Eng. J., 157 (2010) 277–296.
[2] F. Fu, Z. Chen, M. Wang, S. Liu, J. Zhang, R. Han, Q. Xu, Adsorption of methylene blue by a high-efficiency adsorbent (polydopamine microspheres): kinetics, isotherm, thermodynamics and mechanism analysis, Chem. Eng. J., 259 (2015) 53–61.
[3] B. Li, J.Q. Lv, J.Z. Guo, S.Y. Fu, M. Guo, P. Yang, The polyaminocarboxylated modified hydrochar for efficient capturing methylene blue and Cu(II) from water, Bioresour. Technol., 275 (2019) 360–367.
[4] Z. Aksu, I.A. Isoglu, Use of agricultural waste sugar beet pulp for the removal of Gemazol Turquoise Blue-G reactive dye from aqueous solution, J. Hazard. Mater., B137 (2006) 418–430.
[5] M.R. Sohrabi, M. Moghri, H.R.F. Masoumi, S. Amiri, N. Moosavi, Optimization of Reactive Blue 21 removal by nanoscale zero-valent iron using response surface methodology, Arabian J. Chem., 9 (2016) 518–525.
[6] L. Young, Y.U. Jain, Ligninase–catalyzed decolonization, Water Res., 31 (1997) 1187–1193.
[7] S. Wang, Y. Boyjoo, A. Choueib, Z.H. Zhu, Removal of dyes from aqueous solution using fly ash and red mud, Water Res., 39 (2005) 129–138.
[8] S.S. Salih, A. Mahidi, M. Kadhom, T.K. Ghosh, Competitive adsorption of As(III) and As(V) onto chitosan/diatomaceous earth adsorbent, J. Environ. Chem. Eng., 7 (2019) 103407.
[9] S.S. Salih, H.N. Mohammed, G.H. Abdullah, M. Kadhom, T.K. Ghosh, Simultaneous Removal of Cu(II), Cd(II), and Industrial Dye onto a Composite Chitosan Biosorbent, J. Polym. Environ., 28 (2020) 354–365.
[10] S. Chakraborty, S. De, S. DasGupta, J.K. Basu, Adsorption study for the removal of a basic dye: experimental and modelling, Chemosphere, 58 (2005) 1079–1086.
[11] U.B. Deshannavar, G.M. Ratnamala, P.B. Kalburgi, M. El-Harbawi, A. Agarwal, M. Shet, M. Teli, P. Bhandare, Optimization, kinetic and equilibrium studies of Disperse Yellow 22 dye removal from aqueous solutions using Malaysian teak wood sawdust as adsorbent, Indian Chem. Eng., 58 (2016) 12–28.
[12] G.M. Ratnamala, U.B. Deshannavar, S. Munyal, K. Tashildar, S. Patil, A. Shinde, Adsorption of reactive blue dye from aqueous solutions using sawdust as adsorbent: optimization, kinetic, and equilibrium studies, Arabian J. Sci. Eng., 41 (2016) 333–344.
[13] S. Chatterjee, A. Kumar, S. Basu, S. Dutta, Application of response surface methodology for methylene blue dye removal from aqueous solution using low cost adsorbent, Chem. Eng. J., 181–182 (2012) 289–299.
[14] M.S. Reddy, V. Nirmala, C. Ashwini, Bengal gram seed husk as an adsorbent for the removal of dye from aqueous solutions–Batch studies, Arabian J. Chem., 10 (2017) S2554–S2566.
[15] U.J. Etim, S.A. Umoren, U.M. Eduok, Coconut coir dust as a low cost adsorbent for the removal of cationic dye from aqueous solution, J. Saudi Chem. Soc., 20 (2012) S67–S76.
[16] E. El-Ashtoukhy, *Loofa egyptiaca* as a novel adsorbent for removal of direct blue dye from aqueous solution, J. Environ. Manage., 90 (2009) 2755–2761.
[17] M. Ahmaruzzaman, V.K. Gupta, Rice husk and its ash as low-cost adsorbents in water and wastewater treatment, Ind. Eng. Chem. Res., 50 (2011) 13589–13613.
[18] R.A. Fideles, GMD. Ferreira, F.S. Teodoro, OFH. Adarme, L.H.M. da Silva, L.F. Gil, L.V.A. Gurgel, Trimellitated sugarcane bagasse: a versatile adsorbent for removal of cationic dyes from aqueous solution. Part I: Batch adsorption in a monocomponent system, J. Colloid Interface Sci., 515 (2018) 172–188.
[19] L. Hu, Y. Peng, F. Wu, S. Peng, J. Li, Z. Liu, Tubular activated carbons made from cotton stalk for dynamic adsorption of airborne toluene, J. Taiwan Inst. Chem. Eng., 80 (2017) 399–405.
[20] U.B. Deshannavar, B.G. Katageri, M. El-Harbawi, A. Parab, K. Acharya, Fly ash as an adsorbent for the removal of Reactive Blue 25 dye from aqueous solutions: optimization, kinetic and isotherm investigations, P. Est. Acad. Sci., 66 (2017) 336–344.
[21] E. Oguz, Removal of phosphate from aqueous solution with blast furnace slag, J. Hazard. Mater., B114 (2004) 131–137.
[22] C.H. Mei, C. Ting-Chien, P. San-De P, C. Hung-Lung, Adsorption characteristics of Orange II and Chrysophenine on sludge adsorbent and activated carbon fibers, J. Hazard. Mater., 161 (2009) 1384–1390.
[23] K. Fu, Q. Yue, B. Gao, Y. Sun, L. Zhu, Preparation, characterization and application of lignin-based activated carbon from black liquor lignin by steam activation, Chem. Eng. J., 228 (2013) 1074–1082.
[24] S. Vafakhah, M.E. Bahrololoom, R. Bazarganlari, M. Saeedikhan, Removal of copper ions from electroplating effluent solutions with native corn cob and corn stalk and chemically modified corn stalk, J. Environ. Chem. Eng., 2 (2014) 356–361.
[25] T.A. Khan, A. Saif, A., Chaudhry, I., Ali, Equilibrium uptake, isotherm and kinetic studies of Cd(II) adsorption onto iron oxide activated red mud from aqueous solution, J. Mol. Liq., 202 (2014) 165–175.
[26] V.K. Gupta, I., Ali, V.K. Saini, Defluoridation of wastewaters using waste carbon slurry. Water Res., 41 (2007) 3307–3316.
[27] M. Ahmad, S.S. Lee, X. Dou, D. Mohan, J.K. Sung, J.E. Yang, Y.S. Ok, Effects of pyrolysis temperature on soybean stover- and peanut shell-derived biochar properties and TCE adsorption in water, Bioresour. Technol., 118 (2012) 536–544.
[28] A.E. Ofomaja, Y.S. Ho, Effect of temperatures and pH on methyl violet biosorption by Mansonia wood sawdust, Bioresour. Technol., 99 (2008) 5411–5417.
[29] S. Lagergren, Zur theorie der sogenannten adsorption gelöster stoffe [About the theory of so called adsorption of soluble substances], K. Sven. Vetensk. Handl., 24 (1898) 1–39.
[30] Y.S. Ho, G. Mckay, Pseudo-second order model for sorption processes, Process Biochem., 34 (1999) 451–465.
[31] W.J. Weber, J.C. Morris, Kinetics of adsorption on carbon from solutions, J. Sanit. Eng. Div. Am. Soc. Civ. Eng., 89 (1963) 31–60.
[32] I. Langmuir, The adsorption of gases on plane surfaces of glass, mica, and platinum, J. Am. Chem. Soc., 40 (1918) 1361–1368.
[33] G. McKay, H.S. Blair, J.R. Gardner, Adsorption of dyes on chitin, J. Appl. Polym., 27 (1982) 3043–3057.
[34] H. Freundlich, Adsorption in solution, Phys. Chem. Soc., 40 (1906) 1361–1368.
[35] G. McKay, M.S. Otterburn, A.G. Sweeney, The removal of colour from effluent using various adsorbents. III. Silica: rate processes, Water Res., 14 (1980) 15–20.
[36] V.S. Mane, P.V.V. Babu, Kinetic and equilibrium studies on the removal of Congo red from aqueous solution using Eucalyptus wood (*Eucalyptus globulus*) saw dust, J. Taiwan Inst. Chem. Eng., 44 (2013) 81–88.

[37] P. Punjongharn, K. Meevasana, P. Pavasant, Influence of particle size and salinity on adsorption of basic dyes by agricultural waste: dried Seagrape (*Caulerpa lentillifera*), J. Environ. Sci., 20 (2008) 760–768.
[38] Y.S. Ho, G. McKay, The kinetics of sorption of divalent metal ions onto sphagnum moss peat, Water Res., 34 (2000) 735–742.
[39] M.A. Aroua, C.Y. Yin, F.N. Lim, W.L. Kan, W.M. Daud, Effect of impregnation of activated carbon with chelating polymer on adsorption kinetics of Pb^{2+}, J. Hazard. Mater., 166 (2009) 1526–1529.
[40] P. Ndagijimana, X. Liu, Z. Li, Yu. Guangwei, Y. Wang, The synthesis strategy to enhance the performance and cyclic utilization of granulated activated carbon-based sorbent for bisphenol A and triclosan removal, Environ. Sci. Pollut. Res., 27 (2020) 15758–15771.